Neuron
Article

TMC1 and TMC2 Are Components of the Mechanotransduction Channel in Hair Cells of the Mammalian Inner Ear

Bifeng Pan,[1] Gwenaelle S. Géléoc,[1] Yukako Asai,[1] Geoffrey C. Horwitz,[1] Kiyoto Kurima,[2] Kotaro Ishikawa,[2] Yoshiyuki Kawashima,[2] Andrew J. Griffith,[2,*] and Jeffrey R. Holt[1,*]
[1]Department of Otolaryngology, F.M. Kirby Neurobiology Center, Boston Children's Hospital, Harvard Medical School, 300 Longwood Avenue, Center for Life Sciences 12251, Boston, MA 02115, USA
[2]Otolaryngology Branch, National Institute on Deafness and Other Communication Disorders, National Institutes of Health, 5 Research Court, Room 2B-29, Rockville, MD 20850-3320, USA
*Correspondence: griffita@nidcd.nih.gov (A.J.G.), jeffrey.holt@childrens.harvard.edu (J.R.H.)
http://dx.doi.org/10.1016/j.neuron.2013.06.019

SUMMARY

Sensory transduction in auditory and vestibular hair cells requires expression of transmembrane channel-like (*Tmc*) *1* and *2* genes, but the function of these genes is unknown. To investigate the hypothesis that TMC1 and TMC2 proteins are components of the mechanosensitive ion channels that convert mechanical information into electrical signals, we recorded whole-cell and single-channel currents from mouse hair cells that expressed *Tmc1, Tmc2*, or mutant *Tmc1*. Cells that expressed *Tmc2* had high calcium permeability and large single-channel currents, while cells with mutant *Tmc1* had reduced calcium permeability and reduced single-channel currents. Cells that expressed *Tmc1* and *Tmc2* had a broad range of single-channel currents, suggesting multiple heteromeric assemblies of TMC subunits. The data demonstrate TMC1 and TMC2 are components of hair cell transduction channels and contribute to permeation properties. Gradients in TMC channel composition may also contribute to variation in sensory transduction along the tonotopic axis of the mammalian cochlea.

INTRODUCTION

The perception of sound in the mammalian inner ear begins with mechanical deflection of an array of 50–100 modified microvilli, collectively known as the hair bundle. Hair bundles are mechanosensitive organelles that project from the apical surface of inner ear sensory cells. These sensory cells, or hair cells, can respond to subnanometer hair bundle deflections within a few microseconds. Hair cell mechanotransduction is well described by the gating-spring model (Corey and Hudspeth, 1983), which posits that hair bundle deflection stretches elastic elements that directly convey mechanical force to gate mechanosensitive ion channels, located near the tips of hair bundle microvilli (Jaramillo and Hudspeth, 1991; Denk et al., 1995; Lumpkin and Hudspeth, 1995; Beurg et al., 2009).

Several biophysical properties of hair cell transduction vary along the length of the mammalian cochlea, including the conductance of single channels (Beurg et al., 2006) and adaptation of their response to a sustained stimulus (Kennedy et al., 2003). These gradients in transduction properties parallel the tonotopic arrangement of the cochlea and may contribute to the exquisite frequency selectivity of the mammalian inner ear. However, the molecular basis of frequency selectivity within the mammalian cochlea has not been clarified, in part because the mechanosensitive ion channels have not been identified at the molecular level.

Numerous hair cell transduction channel candidates have emerged over the past 15 years, yet none have withstood rigorous scientific scrutiny. Recently, we reported that TMC1 and TMC2 are required for hair cell transduction, raising the possibility that these molecules may be components of the elusive transduction channel (Kawashima et al., 2011), but the data are also consistent with at least two alternate hypotheses: TMC1 and TMC2 may be required for trafficking or development of other hair cell transduction molecules or they may be components of the transduction apparatus, mechanically in series with transduction channels, but not part of the channels themselves (Kawashima et al., 2011).

Tmc1 and *Tmc2* encode six-pass integral membrane proteins with sequence and topology similar to each other (Labay et al., 2010); however, they lack sequence similarity with known ion channels and a pore domain has not been identified. A recent report suggested that *C. elegans tmc-1* forms non-selective cation channels when expressed in heterologous cells (Chatzigeorgiou et al., 2013), though it is unclear if this property extends to other members of the *Tmc* superfamily. While mutations in *TMC1* cause dominant and recessive deafness in humans and mice (Kurima et al., 2002; Vreugde et al., 2002), Marcotti et al. (2006) reported normal mechanotransduction in mouse hair cells that carried either a semidominant *Tmc1* point mutation, known as *Beethoven* (*Bth*), or a recessive in-frame 1.6 kb deletion in *Tmc1*, known as *deafness* (*dn*). They concluded that *Tmc1* is not required for mechanotransduction and that the hearing loss was due to failure of proper hair cell maturation. Kawashima et al. (2011) suggested that expression of a second *Tmc* gene, *Tmc2*, may have accounted for the normal mechanotransduction current amplitudes in the *Tmc1* mutant mice and that the

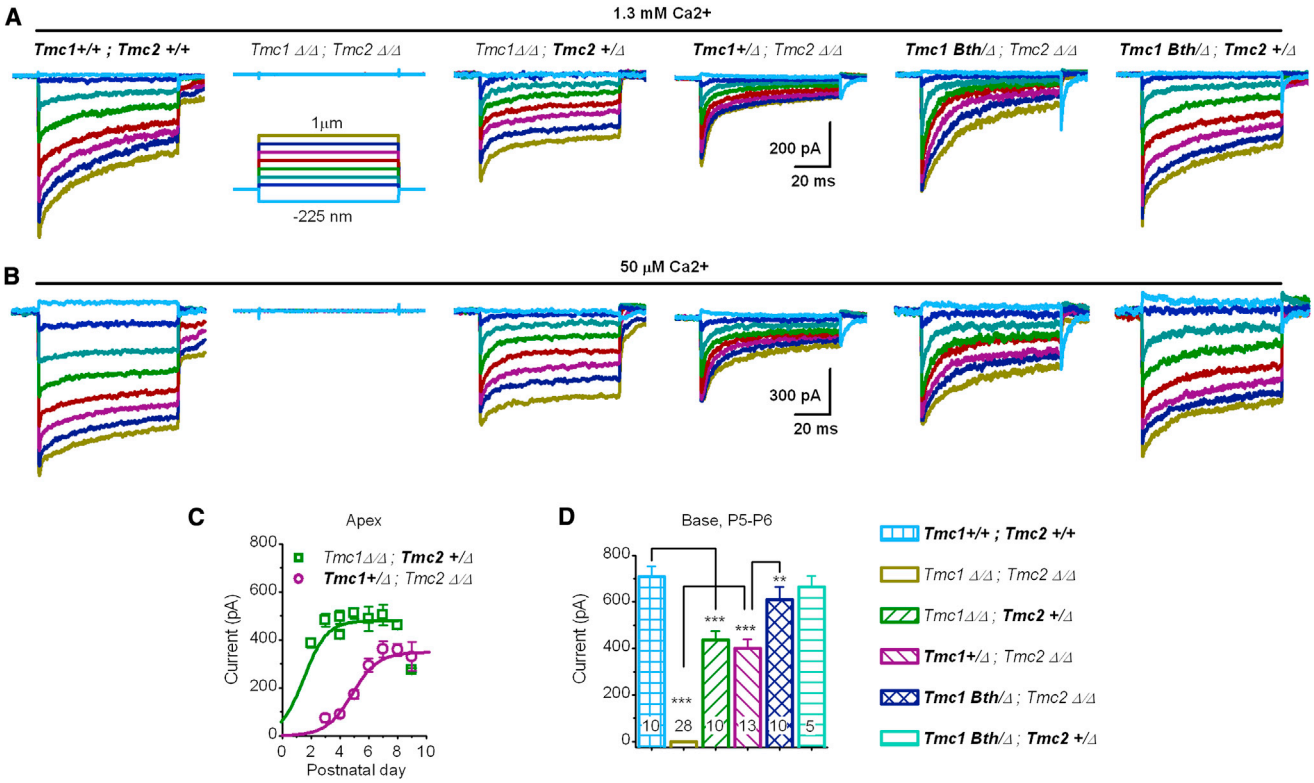

Figure 1. Mechanotransduction Currents Recorded from Cochlear Inner Hair Cells

(A) Representative families of currents recorded at −84 mV from cells of the genotypes indicated above. Cells were from the apical end of P5–P6 cochleas bathed in 1.3 mM Ca^{2+}. The scale bar and stimulus protocol apply to all current families.

(B) Data from the same cells shown in panel A bathed in 50 μM Ca^{2+}, a concentration similar to that of endogenous endolymph.

(C) Mean maximal transduction current amplitudes (±1 SEM) plotted as a function of postnatal age for apical inner hair cells from $Tmc1^{\Delta/\Delta}$;$Tmc2^{+/\Delta}$ (n = 60, ~7/day) and $Tmc1^{+/\Delta}$;$Tmc2^{\Delta/\Delta}$ (n = 48, ~8/day) mice. Data were recorded in 1.3 mM Ca^{2+} at −84 mV and were fitted with smooth curves.

(D) Mean maximal transduction currents (+1 SEM) recorded from basal inner hair cells (P5–P6, 1.3 mM Ca^{2+}, −84 mV).

failure of maturation in *Tmc1*-deficient hair cells was a consequence of a decline in *Tmc2* expression after the first postnatal week. Neither the Marcotti et al. (2006) nor the Kawashima et al. (2011) data could distinguish between a developmental role and a direct role in mechanotransduction. Therefore, to test the hypothesis that TMC1, TMC2, or both are components of the mammalian hair cell transduction channel, we recorded whole-cell and single-channel currents from vestibular type II hair cells and cochlear inner hair cells from mice deficient in *Tmc1*, *Tmc2*, or both, as well as mice that carried the *Bth* mutation in *Tmc1*.

RESULTS AND DISCUSSION

Sensory Transduction in Inner Hair Cells of *Tmc* Mutant Mice

The mammalian cochlea includes three rows of outer hair cells and a single row of inner hair cells. Outer hair cells function to amplify sound stimuli while inner hair cells convey 95% of the afferent information to the brain. In a prior study, we found that *Tmc1* and *Tmc2* are required for mechanotransduction in outer hair cells (Kawashima et al., 2011); inner hair cells were not investigated. To investigate the contributions of *Tmc1* and *Tmc2* to inner hair cell function we recorded whole-cell mechanotransduction currents from mice with targeted deletion alleles of *Tmc1*, *Tmc2*, or both. Hair bundle deflections were evoked using stiff glass probes with tips shaped to fit the concave aspect of bundles of inner hair cell stereocilia. The pipettes were mounted on a stack of piezoelectric actuators that enabled rapid (~50 μs) deflections (Experimental Procedures). We found that inner hair cells deficient in *Tmc1* or *Tmc2* had reduced transduction current amplitudes relative to wild-type cells (Figure 1A). Inner hair cells deficient in both *Tmc1* and *Tmc2* lacked mechanotransduction currents entirely. This was always the case regardless of cochlear region, developmental stage, or extracellular calcium concentration (Figures 1A and 1B). We also noted a developmental delay, with the onset of mechanotransduction in inner hair cells that expressed *Tmc1* occurring about two days later than inner hair cells that expressed *Tmc2* (Figure 1C) and ~2 days later than wild-type mouse outer hair cells (Lelli et al., 2009). The delayed development of mechanotransduction in hair cells that expressed *Tmc1* paralleled the expression pattern of *Tmc1* in wild-type mice (Kawashima et al., 2011). These data extend the conclusion that *Tmc1* and *Tmc2* are required for transduction to include cochlear inner hair cells and confirm that expression of either gene alone is sufficient for transduction.

Since dominant mutations in *TMC1* cause progressive hearing loss in humans and mice (Kurima et al., 2002), we investigated hair cell transduction in *Bth* mice (Vreugde et al., 2002) which express a *Tmc1* point mutation that causes a methionine to lysine substitution at residue 412 (p.M412K). To test the hypothesis that *Bth* mice have normal mechanotransduction during the first postnatal week (Marcotti et al., 2006) due to expression of *Tmc2*, we generated mice with three mutant alleles at the *Tmc1* and *Tmc2* loci by crossing $Tmc1^{Bth}$ onto a *Tmc1;Tmc2*-null background (***Tmc1*^{Bth}** and wild-type alleles are indicated in bold throughout the text and figures to emphasize the identities of the proteins encoded by each genotype). Auditory brainstem responses indicated that the ***Tmc1*$^{Bth/\Delta}$**;$Tmc2^{\Delta/\Delta}$ mice had profound hearing loss (see Figure S1A available online) at 1 month of age, the earliest time point tested. Cell counts from ***Tmc1*$^{Bth/\Delta}$** cochleas at P30–P35 revealed significant inner hair cell loss regardless of the *Tmc2* genotype (Figure S1B). Surprisingly, ***Tmc1*$^{Bth/\Delta}$**;$Tmc2^{\Delta/\Delta}$ hair cells had transduction current amplitudes at P5–P6 that were significantly larger than those of ***Tmc1*$^{+/\Delta}$**;$Tmc2^{\Delta/\Delta}$ mice (Figures 1A, 1B, and 1D), while ***Tmc1*$^{Bth/\Delta}$**;***Tmc2*$^{+/\Delta}$** hair cells had normal mechanotransduction during the first postnatal week (Figures 1A, 1B, and 1D). These data suggest that p.M412K is not a loss-of-function or dominant-negative mutation but must cause deafness due to a gain or change of function. To further explore the differences between $Tmc1^{\Delta/\Delta}$;***Tmc2*$^{+/\Delta}$**, ***Tmc1*$^{+/\Delta}$**;$Tmc2^{\Delta/\Delta}$, and ***Tmc1*$^{Bth/\Delta}$**;$Tmc2^{\Delta/\Delta}$ hair cells, we examined several biophysical properties of hair cell mechanotransduction, including sensitivity, calcium permeability and rate and extent of adaptation. We identified no significant differences in sensitivity (Figure S2) but found striking differences in calcium permeability and adaptation.

To assay calcium permeability we used two electrophysiological measures: Ca^{2+} block and reversal potential. Calcium is a permeant blocker of hair cell transduction channels and reduces the whole-cell mechanotransduction conductance by ~30% in wild-type rat cochlear hair cells (Beurg et al., 2006). To investigate calcium block in ***Tmc1*$^{Bth/\Delta}$**;$Tmc2^{\Delta/\Delta}$ hair cells, we plotted peak transduction currents as a function of voltage and generated mechanotransduction current-voltage (I–V) relations in two different calcium concentrations. Mechanotransduction slope conductance was measured at membrane potentials between −124 and −44 mV in 50 μM Ca^{2+}, a concentration that mimics the endolymph fluid bathing hair bundles, and in normal extracellular Ca^{2+} (1.3 mM). We found an ~40% reduction in slope conductance in ***Tmc1*$^{Bth/\Delta}$**;$Tmc2^{\Delta/\Delta}$ hair cells bathed in 1.3 mM Ca^{2+} relative to 50 μM Ca^{2+}. The ~40% reduction in ***Tmc1*$^{Bth/\Delta}$**;$Tmc2^{\Delta/\Delta}$ cells (Figure S3) was significantly larger ($p < 0.0005$) than the 30% reduction measured in ***Tmc1*$^{+/\Delta}$**;$Tmc2^{\Delta/\Delta}$ cells and $Tmc1^{\Delta/\Delta}$;***Tmc2*$^{+/\Delta}$** cells under the same conditions. Thus, the greater calcium block in the ***Tmc1*$^{Bth/\Delta}$**;$Tmc2^{\Delta/\Delta}$ cells indicates that the p.M412K mutation affects transduction channel permeation properties in *Bth* hair cells.

For the second assay, the cells were bathed in 100 mM external Ca^{2+} with no other permeant cations. The recording pipette contained 140 mM internal Cs^{+} which permitted estimation of the Ca^{2+}/Cs^{+} permeability ratio. We delivered saturating positive and negative step deflections (~1.5 μm range) and simultaneous voltage steps to inner hair cells of the three genotypes (Figures 2A–2C). Peak transduction currents were plotted as a function of voltage (Figure 2D). We found a substantial negative shift in the I-V curve reversal potentials for ***Tmc1*$^{Bth/\Delta}$**;$Tmc2^{\Delta/\Delta}$ hair cells, relative to ***Tmc1*$^{+/\Delta}$**;$Tmc2^{\Delta/\Delta}$ cells. Reversal potentials, measured from the x-intercept of the I–V curves, indicated a difference of ~13 mV (Figure 2E) between hair cells of the two genotypes. Inner hair cells of $Tmc1^{\Delta/\Delta}$;***Tmc2*$^{+/\Delta}$** mice had more positive reversal potentials (Figures 2D and 2E) consistent with recent measurements from outer hair cells of mice that carried the recessive *deafness* mutation in *Tmc1* (Kim and Fettiplace, 2013).

We used our reversal potential data together with the Goldman-Hodgkin-Katz equation to estimate the calcium permeability ratio relative to internal cesium. We found that TMC2-expressing cells had higher calcium selectivity than TMC1-expressing cells (Figure 2F) consistent with inner hair cell data from Kim and Fettiplace (2013). Importantly, we found that the p.M412K point mutation in $TMC1^{Bth}$ -expressing cells

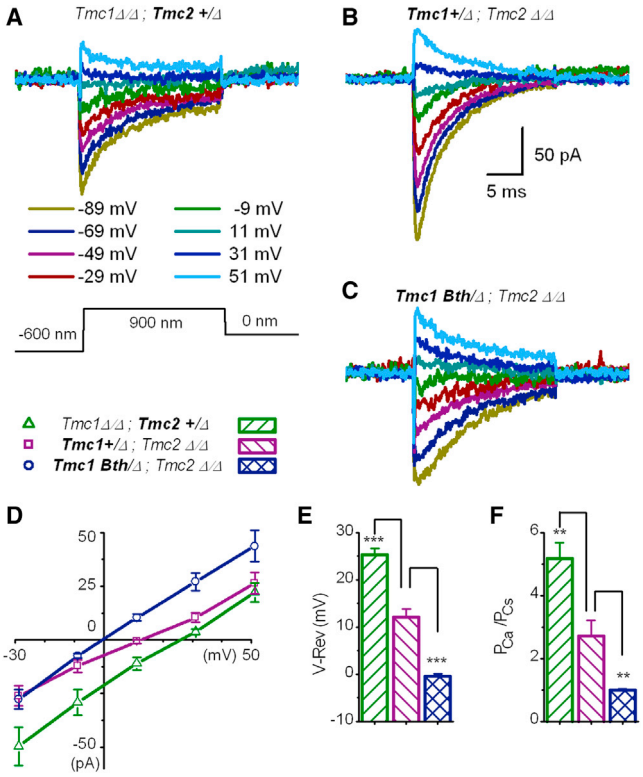

Figure 2. Whole-Cell Mechanotransduction Current-Voltage Relationships Measured in 100 mM Calcium

(A–C) Representative families of currents recorded at the step potentials shown below (A) from inner hair cells of the genotypes indicated. A mechanical stimulus (protocol shown at the bottom of A) that evoked hair bundle deflections from −0.6 μm to 0.9 μm was superimposed on the voltage steps. The scale bar in (B) applies to (A)–(C).

(D) Mean (± 1 SEM) current-voltage relations taken from the peak transduction currents shown in (A)–(C) for eight cells of each genotype.

(E) Mean (+ 1 SEM) reversal potentials measured from the x-intercept of individual I–V curves generated from eight cells of each genotype.

(F) Mean (+ 1 SEM) calcium permeability ratios relative to cesium calculated using the Goldman-Hodgkin-Katz equation and the reversal potentials shown in (E).

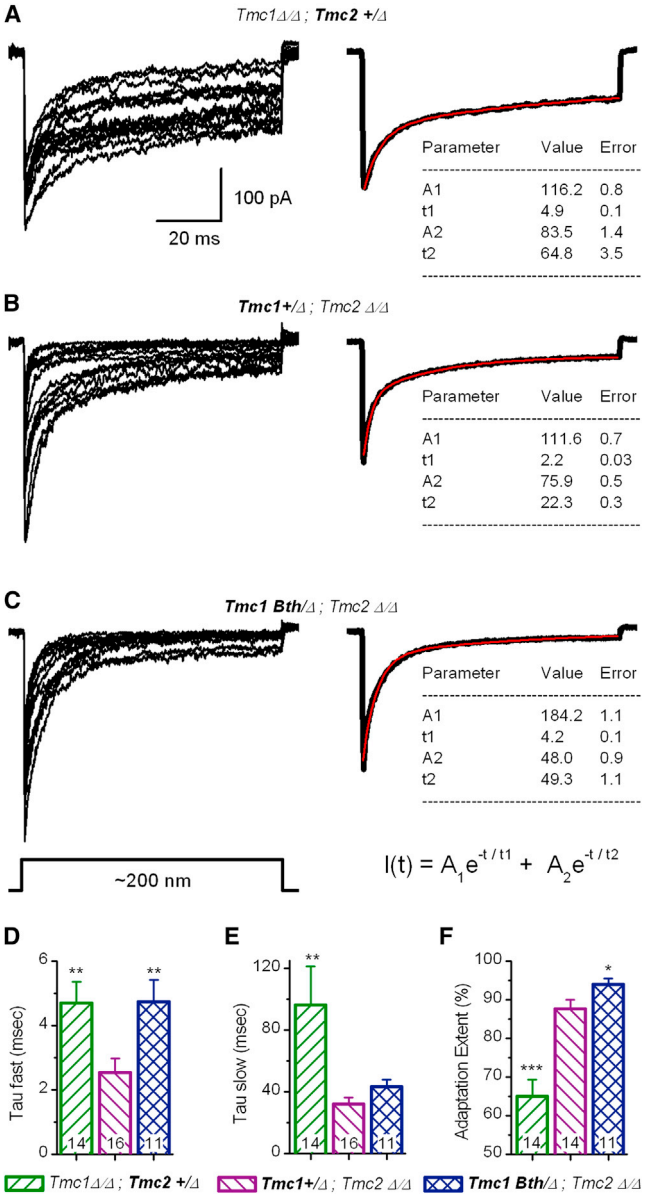

Figure 3. Analysis of Transducer Adaptation in *Tmc* Mutant Hair Cells Recorded in 50 μM Ca^{2+}

(A–C) Whole-cell mechanotransduction currents (left) recorded from inner hair cells of $Tmc1^{\Delta/\Delta}$;$Tmc2^{+/\Delta}$ (n = 14 cells), $Tmc1^{+/\Delta}$;$Tmc2^{\Delta/\Delta}$ (n = 16 cells) and $Tmc1^{Bth/\Delta}$;$Tmc2^{\Delta/\Delta}$ (n = 11 cells) mice as indicated above. The scale bar applies to all panels. Traces were selected as the 50% maximal current from families evoked by mechanical stimuli that spanned the sensitive range for each cell. Each trace was fitted with a double exponential equation (bottom right) that yielded fast (t1) and slow (t2) time constants. The extent of adaptation was calculated as the residual current at the end of the step divided by the peak current. All traces shown on the left were averaged to generate the composite traces on the right (black line) and were fitted with the double exponential equation. The fit parameters are shown below each trace.

(D) Mean (+1 SEM) fast adaptation time constants measured in 50 μM Ca^{2+} for the individual current traces shown in (A)–(C).

(E) Mean (+1 SEM) slow adaptation time constants.

(F) Mean (+1 SEM) extent of adaptation measured as the residual current at the end of a 90-msec step divided by the peak current. Number of cells is shown at the bottom. Statistical significance relative to $Tmc1^{+/\Delta}$;$Tmc2^{\Delta/\Delta}$ is indicated: ***p < 0.001, **p < 0.01, *p < 0.05.

caused a significant reduction in calcium selectivity relative to TMC1-expressing cells (Figure 2F). Thus, the p.M412K mutation in TMC1 alters a core property of the mechanically evoked transduction current—its calcium permeability—supporting the hypothesis that TMC1 is an integral component of the hair cell transduction channel.

Since hair cell adaptation is calcium-sensitive (Eatock et al., 1987; Assad and Corey, 1992; Ricci and Fettiplace, 1997; Kennedy et al., 2003; Farris et al., 2006) we wondered whether differences in calcium permeability in *Tmc* mutant hair cells might affect adaptation. We measured adaptation time constants and extent from cells bathed in endolymph calcium concentrations (50 μM; Figure 1B). Current traces with half-maximal peak amplitudes were fitted with double exponential equations (Figure 3). The fits extended from the peak of the inward current to the end of the mechanical step (Figures 3A–3C, right, red traces). We found that the fast component of adaptation was significantly faster in $Tmc1^{+/\Delta}$;$Tmc2^{\Delta/\Delta}$ hair cells than in $Tmc1^{\Delta/\Delta}$;$Tmc2^{+/\Delta}$ or $Tmc1^{Bth/\Delta}$;$Tmc2^{\Delta/\Delta}$ cells (Figure 3D). The slow component of adaptation was slower in $Tmc1^{\Delta/\Delta}$;$Tmc2^{+/\Delta}$ cells than either $Tmc1^{+/\Delta}$;$Tmc2^{\Delta/\Delta}$ or $Tmc1^{Bth/\Delta}$;$Tmc2^{\Delta/\Delta}$ cells (Figure 3E). The extent of adaptation also varied among the three genotypes (Figure 3F). The differences in fast adaptation time constants may be a consequence of different calcium permeabilities (Figure 2F) or they may reflect inherent differences in the adaptation properties of TMC proteins. Wu et al. (1999) modeled adaptation in auditory hair cells and suggested that fast adaptation required a calcium binding site in close proximity to the channel pore. Thus, it is plausible that amino acid sequence differences between TMC1 and TMC2 may contribute to the different fast adaptation properties reported here. Because slow adaption is thought to involve myosin motors (Holt et al., 2002) at a remote location (Wu et al., 1999), minor changes in calcium entry in cells bathed in 50 μM calcium may have little impact on the local calcium concentration at the slow adaptation site due to diffusion and the activity of calcium pumps and buffers.

Single-Channel Properties of *Tmc* Mutant Inner Hair Cells

Another core property of an ion channel is its single-channel conductance. To examine contributions of TMC proteins to the properties of single transduction channels we designed a stimulation and recording paradigm. Inner hair cell bundles consist of an array of loosely organized stereocilia, with few lateral connections and the tallest row towering above the rest. To exploit this morphology, we engineered stimulus pipettes that tapered to a few hundred nanometers in diameter at their distal tips which we used to deflect single stereocilia (Figure S4). We recorded the response of single stereocilium deflections in whole-cell mode at a holding potential of −84 mV. At this potential, voltage-dependent sodium and calcium channels were deactivated and we substituted Cs^+ for K^+ in the recording pipette to block residual potassium currents. The cells were bathed in an endolymph concentration of calcium, 50 μM, which had the

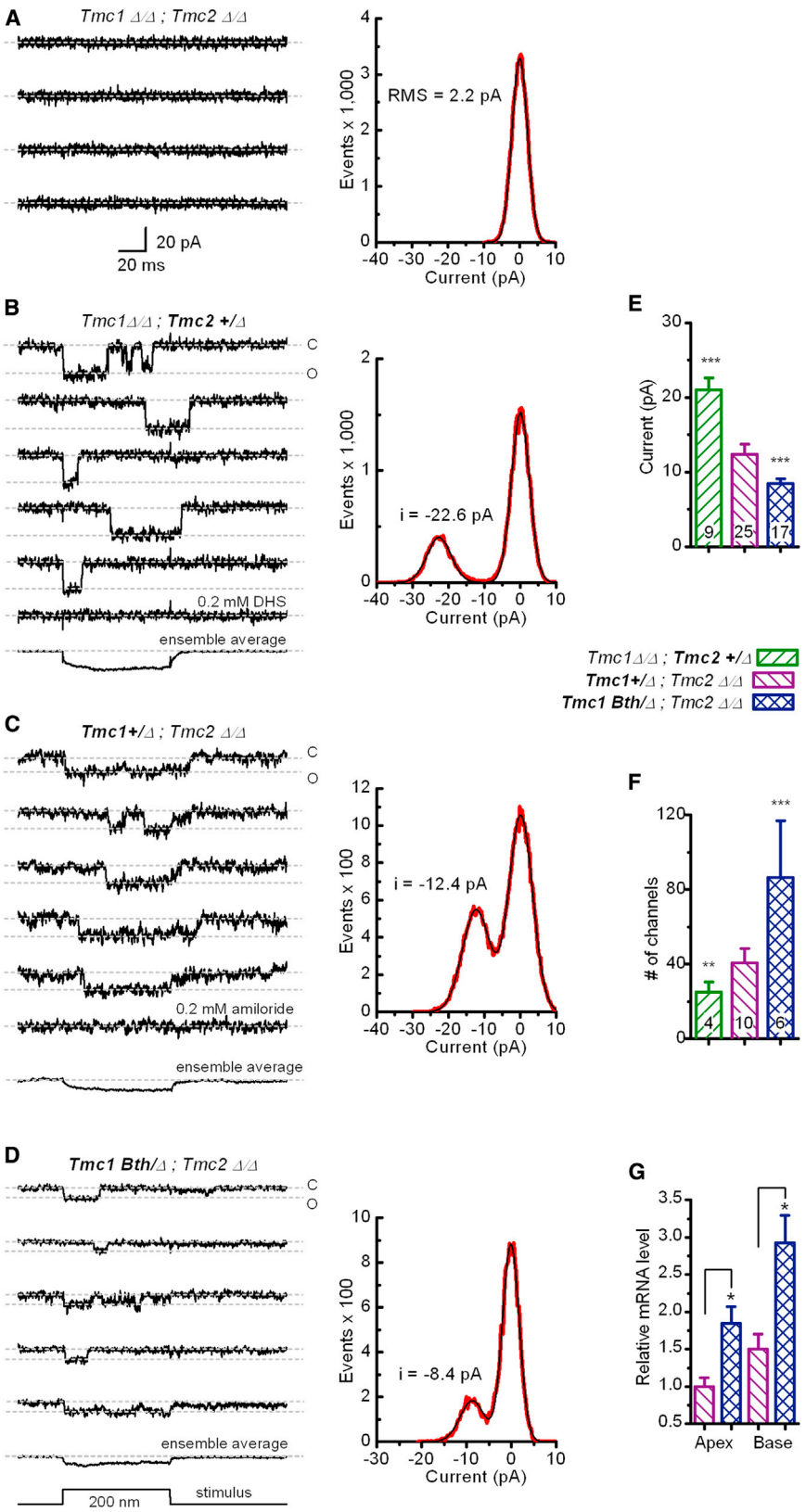

Figure 4. Single-Channel Events Recorded from Inner Hair Cells of *Tmc* Mutant Mice

(A) To evaluate the recording paradigm, the noise floor was measured at −84 mV from a P4 basal IHC excised from a $Tmc1^{\Delta/\Delta};Tmc2^{\Delta/\Delta}$ mouse. Four representative traces are shown. Dashed lines indicate the zero current level. The stimulus protocol is shown at the bottom. The scale bar applies all current traces. Each trace was used to generate an event histogram (right, red trace). The data were fitted with a Gaussian equation which had a peak at 0.07 pA and a width of 4.3 pA (black).

(B) Single-channel currents recorded in 50 μM Ca^{2+} from a P2 $Tmc1^{\Delta/\Delta};\mathbf{Tmc2}^{+/\Delta}$ basal inner hair cell. Rapid current steps were frequently noted. Open and closed states are indicated at the right of the first of five representative traces. Application of 0.2 mM dihydrostreptomycin (DHS) eliminated all single-channel events (bottom). The ensemble average of 43 traces containing step transitions show the responses were linked to the mechanical stimulus. The event histogram (right, red trace) was fitted with the sum of two Gaussian curves (black trace) that had peaks at −0.02 pA and −22.6 pA with widths of 5.0 and 6.7 pA, respectively.

(C) Five representative traces recorded in 50 μM Ca^{2+} from a basal, P4 $\mathbf{Tmc1}^{+/\Delta};Tmc2^{\Delta/\Delta}$ inner hair cell. 0.2 mM amiloride, an alternate transduction channel blocker (Rüsch et al., 1994), eliminated all single-channel events (bottom). An ensemble average of 50 traces is shown below. The event histogram (right) was fitted with the sum of two Gaussians with peaks of 0.1 and −12.3 pA and widths of 6.6 and 7.6 pA, respectively.

(D) Representative traces recorded in 50 μM Ca^{2+} from a P5 basal hair cell excised from a $\mathbf{Tmc1}^{\mathbf{Bth}/\Delta};Tmc2^{\Delta/\Delta}$ mouse. An ensemble average of 22 traces and the stimulus protocol are shown at the bottom. Gaussian fits to the event histogram had peaks at −0.2 and −8.6 pA with widths of 3.7 and 5.9 pA.

(E) Mean (+1 SD) single-channel currents recorded from 51 inner hair cells from all regions of the cochlea and developmental stages between P0 and P9 (n = 19 mice). The stars (***) indicate highly significant differences relative to $\mathbf{Tmc1}^{+/\Delta};Tmc2^{\Delta/\Delta}$ cells: $p < 1e^{-10}$.

(F) Whole-bundle currents recorded in 50 μM Ca^{2+} were divided by the mean single-channel currents shown in (E) to yield an estimate of the number of transduction channels for 20 cells. Mean (+ 1 SD) number of channels/cell for each genotype is indicated, revealing significantly more functional channels in the $\mathbf{Tmc1}^{\mathbf{Bth}/\Delta};Tmc2^{\Delta/\Delta}$ hair cells. ***$p < 0.001$, **$p < 0.01$.

(G) Representative quantitative RT-PCR data for *Tmc1* mRNA selected from three biological replicates each of which yielded similar results. Messenger RNA was harvested from the apical and basal portions of P5 mouse cochleas excised from $\mathbf{Tmc1}^{+/\Delta};Tmc2^{\Delta/\Delta}$ and $\mathbf{Tmc1}^{\mathbf{Bth}/\Delta};Tmc2^{\Delta/\Delta}$ mice. Data were normalized relative to *Actb* and *Tmc1* levels from the apical $\mathbf{Tmc1}^{+/\Delta};Tmc2^{\Delta/\Delta}$ sample using the ΔΔCt method. The mean (+1 SD) of three technical replicates are shown. *$p < 0.05$.

dual effect of enhancing transduction current amplitudes relative to standard extracellular calcium (i.e., minimizing calcium block) and prolonging channel open times by reducing calcium-dependent adaptation.

We began with a characterization of *Tmc1*$^{\Delta/\Delta}$;*Tmc2*$^{\Delta/\Delta}$ cells which lacked single-channel currents entirely and thus permitted evaluation of the recording paradigm in a quiescent background (Figure 4A). We observed no voltage-dependent or ligand-gated ion channel activity. Under these conditions the root mean square (RMS) noise was 2.2 pA, which we reasoned would allow us to resolve currents with amplitudes greater than 4.4 pA. When we used this technique to record from *Tmc1*$^{\Delta/\Delta}$;***Tmc2***$^{+/\Delta}$ inner hair cells, we observed prominent single-channel currents (Figure 4B) in response to small stereocilium deflections. The single-channel events were blocked by application of 0.2 mM dihydrostreptomycin (DHS), a hair cell transduction antagonist (Marcotti et al., 2005). Ensemble averages of 20–50 traces revealed that the unitary currents coincided with stereocilium step deflections. The data were binned (0.3 pA bin width) into amplitude histograms which revealed two prominent peaks centered at the zero current level (closed state) and at −22 pA, the presumed open channel current for a single transduction channel.

Tmc1$^{+/\Delta}$;*Tmc2*$^{\Delta/\Delta}$ inner hair cells had unitary current steps that were significantly smaller (Figure 4C). The current amplitudes were −10 to −12 pA, about half that measured from *Tmc1*$^{\Delta/\Delta}$; ***Tmc2***$^{+/\Delta}$ hair cells. We recorded from 25 ***Tmc1***$^{+/\Delta}$;*Tmc2*$^{\Delta/\Delta}$ and nine *Tmc1*$^{\Delta/\Delta}$;***Tmc2***$^{+/\Delta}$ inner hair cells from all regions of the cochlea, throughout the first postnatal week and found little variation in current amplitude for a given genotype (Figure 4E). In some recordings, we noticed spontaneous single-channel events that had amplitudes similar to those of the mechanically evoked currents (Figures S5A and S5C). Occasionally, we observed current steps that were two (Figure S5B) or three times the unitary value, possibly reflecting gating of two or three channels within an intact column of two to three stereocilia (Figure S4B). There were also several recordings in which adaptation was prominent for both positive and negative deflections (Figure S6). Ensemble averages revealed single-channel adaptation that had time courses and extents of adaptation similar to the macroscopic currents recorded in low Ca^{2+} from inner hair cells of equivalent *Tmc* genotypes. Whether the differences in single-channel adaptation are a consequence of the different calcium permeability, inherent differences in the properties of TMC proteins or both is unclear.

Next, we recorded from mutant mice that expressed the $TMC1^{Bth}$ protein and found that the p.M412K mutation in TMC1 had a significant effect on the amplitude of the single-channel currents (Figure 4D). Unitary currents measured from 17 ***Tmc1***$^{Bth/\Delta}$;*Tmc2*$^{\Delta/\Delta}$ inner hair cells were reduced by ~33% relative to those recorded from cells with a single wild-type allele of *Tmc1* (Figure 4E). The change in unitary current amplitude resulting from a point mutation in TMC1 provides compelling evidence that TMC1 is a component of the hair cell transduction channel.

To calculate the number of channels/cell we compared the single-channel current amplitudes to the macroscopic currents for hair cells of the same genotype. We found that the ***Tmc1***$^{Bth/\Delta}$;*Tmc2*$^{\Delta/\Delta}$ cells expressed over twice the number of functional channels as either of the other two genotypes (Figure 4F). ***Tmc1***$^{Bth/\Delta}$;*Tmc2*$^{\Delta/\Delta}$ cells had a mean of 86 channels/cell. Estimates of the number of tip-links range from 50 to 100 per cell depending on the number of stereocilia. Thus, the ***Tmc1***$^{Bth/\Delta}$;*Tmc2*$^{\Delta/\Delta}$ cells had 1-2 channels per tip-link on average. ***Tmc1***$^{+/\Delta}$;*Tmc2*$^{\Delta/\Delta}$ cells had 40 channels/cell and *Tmc1*$^{\Delta/\Delta}$;***Tmc2***$^{+/\Delta}$ cells had 25, suggesting that not all tip-link sites were occupied, perhaps due to haploinsufficiency. To investigate whether the difference in the number of transduction channels between ***Tmc1***$^{+/\Delta}$;*Tmc2*$^{\Delta/\Delta}$ and ***Tmc1***$^{Bth/\Delta}$;*Tmc2*$^{\Delta/\Delta}$ hair cells was due to changes in gene expression, we performed a quantitative RT-PCR analysis using cochlear tissue harvested from ***Tmc1***$^{+/\Delta}$;*Tmc2*$^{\Delta/\Delta}$ and ***Tmc1***$^{Bth/\Delta}$;*Tmc2*$^{\Delta/\Delta}$ mice. The analysis revealed significantly higher *Tmc1* mRNA expression in *Bth* mice (Figure 4G), which may account for the larger whole-cell transduction currents in these mice. The mechanism for altered *Tmc1* gene expression and eventual hair cell death in the *Bth* mice is unclear. However, recent evidence shows that proper calcium homeostasis is required for hair cell survival (Esterberg et al., 2013), raising the possibility that altered calcium permeability in *Bth* mice may lead to hair cell degeneration and deafness (Figure S1B). A similar mechanism may underlie dominant, progressive hearing loss in DFNA36 patients who carry a point mutation (p.G417R) in an adjacent residue in the human TMC1 ortholog (Yang et al., 2010).

Wild-Type Inner Hair Cells Have a Range of Single-Channel Properties

Next, we measured single-channel currents in wild-type inner hair cells at time points when both *Tmc1* and *Tmc2* were expressed (Figure 5). During the first postnatal week we recorded a range of unitary current amplitudes from all regions of the cochlea that was significantly broader than that observed in *Tmc* mutant mice. Representative examples that span the range are shown in Figures 5A–5C. Unitary current values were divided by driving force (84 mV based on a 0 mV reversal potential in 50 μM Ca^{2+}, see Figure S3) to calculate single-channel conductance (*g*). In wild-type mouse inner hair cells, *g* ranged between 60 and 330 pS during the first postnatal week. These values encompass the wide range of single-channel conductances reported for auditory hair cells of various species (Crawford et al., 1991; Géléoc et al., 1997; Ricci et al., 2003; Beurg et al., 2006). Figure 5D shows a scatter plot of 44 single-channel conductances measured from wild-type cells, along with measurements from 18 ***Tmc1***$^{+/\Delta}$;*Tmc2*$^{\Delta/\Delta}$ and *Tmc1*$^{\Delta/\Delta}$;***Tmc2***$^{+/\Delta}$ cells. The data from the *Tmc* mutant mice are tightly clustered relative to the wild-type data which are more broadly distributed. To examine the possibility that the wild-type data form discrete groups we performed a cluster analysis using three statistical tests (Experimental Procedures) each of which reported that the data are best described by four clusters. The mean value for each cluster is indicated by the straight lines (Figure 5D). Together, these data reveal that both ***Tmc1***$^{+/\Delta}$;*Tmc2*$^{\Delta/\Delta}$ and *Tmc1*$^{\Delta/\Delta}$;***Tmc2***$^{+/\Delta}$ hair cells have transduction channels with relatively homogeneous single-channel properties, whereas wild-type hair cells that express both *Tmc1* and *Tmc2* display significant heterogeneity. The data support a model in which

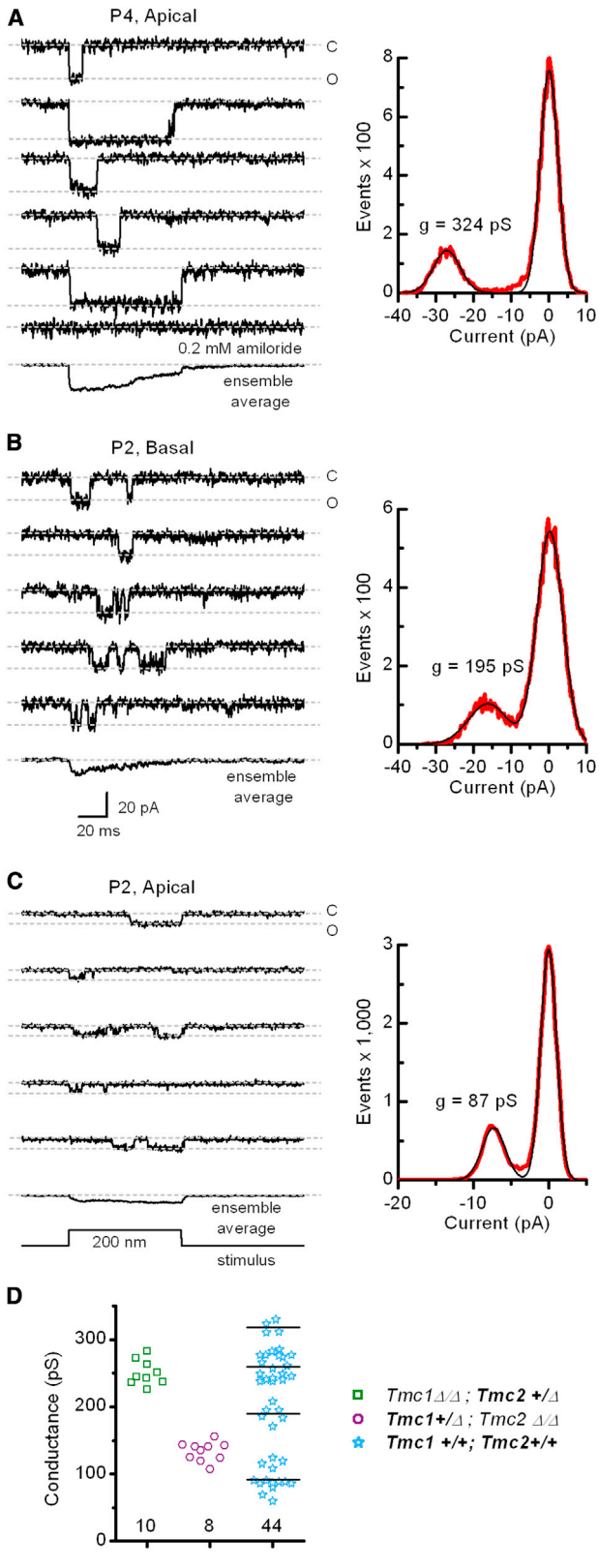

Figure 5. Single-Channel Events Recorded from Wild-Type Inner Hair Cells

(A) Five representative traces recorded from a wild-type P4 apical hair cell that illustrate a mechanotransduction channel at the upper end of the single-channel conductance range. The currents were blocked by 0.2 mM amiloride (bottom). An ensemble average of 24 traces is shown below. The event histogram (right, red trace) was fitted with two Gaussian functions (black trace) with peaks at 0 and −27.2 pA and widths of 4.8 and 7.1 pA. Single-channel conductance was calculated as current/driving force, the latter equal to the difference between the holding potential (−84 mV) and the reversal potential (0 mV in 50 μM Ca^{2+}; from Figure S3).

(B) Representative traces recorded from a wild-type basal hair cell at P2. The single-channel current amplitude was in the middle range of 44 channels examined. An ensemble average of 44 traces is shown at the bottom. The event histogram (right) was fitted with two Gaussians with peaks at 0.2 and −16.2 pA and widths of 6.9 and 10.4 pA. The scale bar at the bottom applies to all current traces.

(C) Traces recorded from a wild-type apical hair cell at P2 that represent the lower end of the single-channel conductance range. An ensemble average of 35 traces is shown at the bottom. The histogram (right) was fitted with two Gaussians with peaks of 0 and −7.3 pA and widths of 2.1 and 3.1, respectively.

(D) Scatter plot of single-channel conductance for $Tmc1^{\Delta/\Delta}$;$\mathbf{Tmc2}^{+/\Delta}$, $\mathbf{Tmc1}^{+/\Delta}$;$Tmc2^{\Delta/\Delta}$ and wild-type transduction channels recorded from inner hair cells during the first postnatal week. Note the wild-type values cluster in four discrete groups. The mean for each group is indicated by the horizontal line. Number of measurements for each genotype is indicated below.

TMC1 and TMC2 can contribute to homomeric transduction channels and when coexpressed in wild-type cells can coassemble to form heteromeric channels with a range of discrete conductance levels, including conductance levels that are larger than either TMC1 or TMC2 homomers. Whether other single-channel properties, such as kinetics, calcium permeability, or adaptation vary as a function of subunit composition remains to be determined.

Since both the single-channel and the whole-cell transduction data in *Tmc* mutant mice reveal distinct biophysical properties, we suggest that prior published data on hair cell mechanotransduction, particularly during early developmental stages, may need to be reinterpreted with regard to the complex *Tmc* spatiotemporal expression patterns and the developmental switch from *Tmc2* to *Tmc1* in cochlear hair cells (Kawashima et al., 2011). Indeed, the maturation of mechanotransduction properties in cochlear outer hair cells that occurs throughout the first postnatal week (Waguespack et al., 2007; Lelli et al., 2009) may be the consequence of dynamic *Tmc1* and *Tmc2* expression patterns.

Tmc Function in Vestibular Hair Cells

Lastly, we wondered whether the same general properties we found in cochlear inner hair cells of *Tmc* mutant mice can be generalized to other hair cell types. To investigate this we recorded single-channel and whole-cell transduction currents from vestibular hair cells of the mouse utricle. In type II vestibular hair cells bathed in 1.3 mM Ca^{2+}, single-channel conductances from $Tmc1^{\Delta/\Delta}$;$\mathbf{Tmc2}^{+/\Delta}$ mice (mean = 101 ± 18 pS, n = 3; Figure 6A) were about twice the amplitude of those recorded from $\mathbf{Tmc1}^{+/\Delta}$;$Tmc2^{\Delta/\Delta}$ mice (mean = 50 ± 18 pS, n = 4; Figure 6B). In wild-type cells (Figure 6C), most single-channel events had large conductances (mean = 114 ± 8 pS, n = 3), consistent with our previous data showing that *Tmc2* is highly expressed

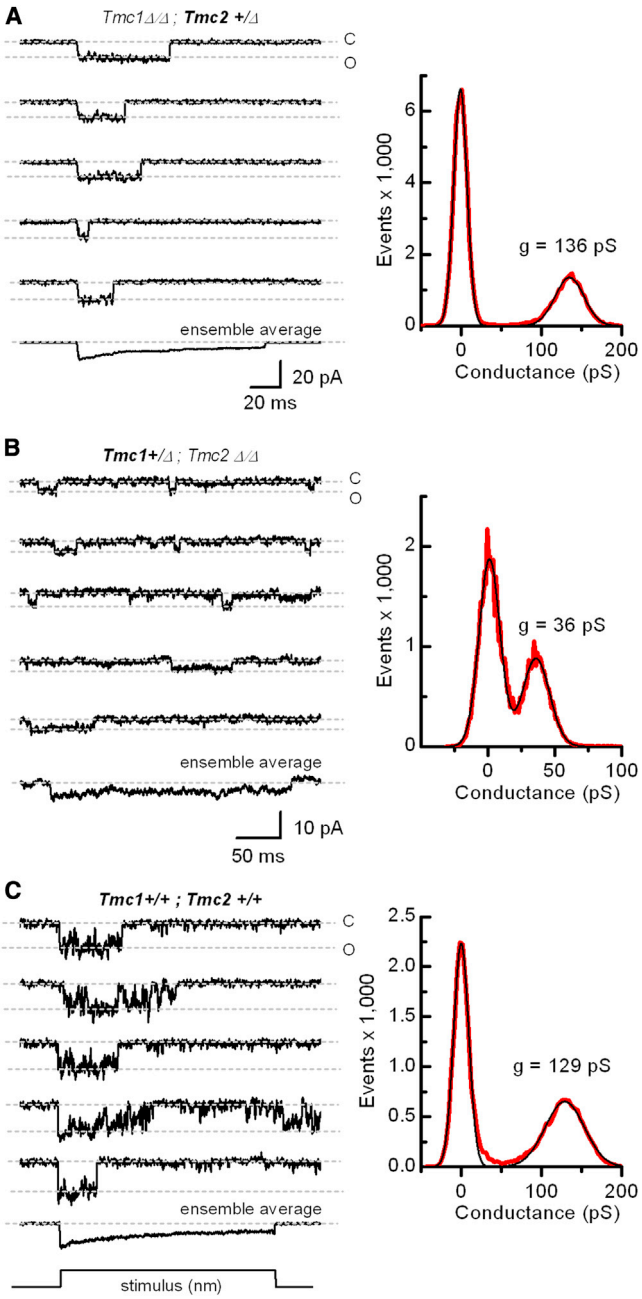

Figure 6. Transduction Currents Recorded from Vestibular Type II Hair Cells of Wild-Type and *Tmc* Mutant Mice

(A) Representative single-channel events recorded from a utricle type II hair cell acutely excised from a $Tmc1^{\Delta/\Delta}$;$\mathbf{Tmc2}^{+/\Delta}$ mouse at P7. An ensemble average of 31 traces is shown at the bottom. To estimate single-channel conductance, an event histogram (right, red trace) was generated and the current values were divided by driving force (−94 mV). The Gaussian curves (black line) had peaks at 0 and 136 pS and widths of 16.7 and 36.5 pS. The scale bar applies to all traces.

(B) Single-channel events recorded from a utricle type II hair cell acutely excised from a $\mathbf{Tmc1}^{+/\Delta}$;$Tmc2^{\Delta/\Delta}$ mouse at P4. An ensemble average of 22 traces is shown at the bottom. Single-channel currents were divided by driving force (−94 mV) and plotted in an event histogram (right, red trace). The data were fitted with two Gaussian curves (black lines) that had peaks at 0 and 36 pS and widths of 15.7 and 20.4 pS. The scale bar applies to all traces in (B) and (C).

(C) Currents recorded from a wild-type utricle type II cell at P0. Ensemble average = 60 traces. Single-channel currents were divided by driving force (−84 mV) and plotted in the histogram (right, red trace). Gaussian curves (black line) had peaks at 0 and 129 pS and widths of 18.7 and 49 pS.

in vestibular hair cells during the first postnatal week (Kawashima et al., 2011) Although the single-channel conductances measured in vestibular cells were smaller than those of inner hair cells, this is likely the result of the elevated extracellular calcium (1.3 mM) required for the vestibular cell recording paradigm. This is the first report of direct measurement of single-channel currents from vestibular hair cells of any species, though we note that the single-channel conductances we measured from $\mathbf{Tmc1}^{+/\Delta}$;$Tmc2^{\Delta/\Delta}$ mouse utricle hair cells are similar to those of a prior noise analysis estimation from bullfrog saccular hair cells (Holton and Hudspeth, 1986).

In both auditory and vestibular hair cells, the amplitude of the single-channel conductance in TMC2-expressing cells was approximately double that of TMC1-expressing cells. The larger conductance in TMC2-expressing cells raises an intriguing possibility regarding the developmental switch from *Tmc2* to *Tmc1* that occurs at the end of the first postnatal week (Kawashima et al., 2011). Development of the endocochlear potential (+80 mV in the endolymphatic space that bathes auditory hair bundles) occurs just prior to the onset of hearing at P10–P12 in mice (Steel and Barkway, 1989), and coincides with the switch from high-conductance TMC2 transduction channels to low-conductance TMC1 channels. We hypothesize that acquisition of low-conductance TMC1 channels is offset by development of the endocochlear potential which provides a steep electrochemical gradient that drives sensory transduction in the mature mammalian auditory organ. For example, a 265-pS TMC2 channel will pass ~17 pA of current at a resting potential of −64 mV during the first postnatal week. This is approximately equal to the current passed by a 120-pS TMC1 channel with a 144 mV driving force (difference between the −64 mV resting potential and the +80 mV endocochlear potential) during the second postnatal week. Thus, the counterbalance between the high- to low-conductance switch and development of the endocochlear potential may function to ensure stable transduction current amplitudes during development and into adulthood. Interestingly, vestibular organs, which lack an endolymphatic potential, retain expression of *Tmc2*, and presumably high-conductance transduction channels, into adulthood.

To test the hypothesis that coexpression of *Tmc1* and *Tmc2* can give rise to a range of transduction properties in vestibular hair cells we overexpressed *Tmc2* in $\mathbf{Tmc1}^{+/\Delta}$;$Tmc2^{\Delta/\Delta}$ hair cells using adenoviral expression vectors. Relative to $\mathbf{Tmc1}^{+/\Delta}$;$Tmc2^{\Delta/\Delta}$ hair cells (Figure 7A) and $\mathbf{Tmc1}^{+/\Delta}$;$Tmc2^{\Delta/\Delta}$ cells transfected with Ad-*Tmc1* (Figure 7B), we found that $\mathbf{Tmc1}^{+/\Delta}$;$Tmc2^{\Delta/\Delta}$ cells transfected with Ad-*Tmc2* had significantly larger transduction currents, almost −400 pA in the example shown in Figure 7C. Data from 26 cells (Figure 7D) show that $\mathbf{Tmc1}^{+/\Delta}$;$Tmc2^{\Delta/\Delta}$ cells transfected with Ad-*Tmc2* had significantly larger mean maximal currents (−246 pA) than the sum of the mean maximal currents from cells that express

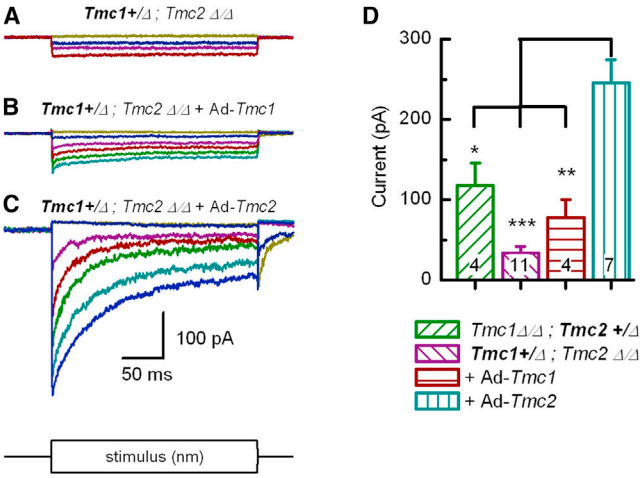

Figure 7. Whole-Cell Mechanotransduction Currents Recorded at –64 mV from Control Type II Hair Cells and Cells Exposed to Adenoviral Vectors

(A–C) Families of whole-cell currents recorded from ***Tmc1***$^{+/\Delta}$;*Tmc2*$^{\Delta/\Delta}$ vestibular hair cells under control conditions (A) or following exposure to Ad-*Tmc1* and 5 days in culture (B) or exposure to Ad-*Tmc2* and 4 days in culture (C). The scale bar at the bottom applies to all current families.

(D) Bar graph summarizing the mean (+1 SEM) maximal whole-cell transduction currents for the conditions indicated below. Number of cells is shown for each bar. Statistical significance relative to the condition on the far right is indicated according to ***p < 0.001, **p < 0.01, *p < 0.05.

either TMC1 or TMC2 alone (−34 + −118 = −152 pA). The currents from ***Tmc1***$^{+/\Delta}$;*Tmc2*$^{\Delta/\Delta}$ cells transfected with Ad-*Tmc2* were also significantly larger than *Tmc1*$^{\Delta/\Delta}$;*Tmc2*$^{\Delta/\Delta}$ cells transfected with Ad-*Tmc2* (−136 pA; Kawashima et al., 2011). This result demonstrates that coexpression of *Tmc1* and *Tmc2* can contribute to larger transduction currents than can be explained by the sum of overexpression of either *Tmc1* or *Tmc2* alone. Distinct channel properties in cells that express two ion channel genes relative to those that express either gene alone is evidence that the channel subunits can co-assemble to form ion channels with unique properties (Kubisch et al., 1999).

Conclusions

Our data support the hypothesis that TMC1 and TMC2 are components of the mechanotransduction channel in auditory and vestibular hair cells of the mammalian inner ear. The strongest evidence is derived from the mutant mice that express the *Tmc1*^{Bth} allele in the absence of wild-type *Tmc1* and *Tmc2*. The reduced single-channel current levels and the reduced calcium permeability that result from the p.M412K point mutation in *Tmc1* implicate TMC1 as a pore-forming subunit of the transduction channel. A similar line of evidence has been used to identify mechanosensitive channels in worms (O'Hagan et al., 2005; Kang et al., 2010) and fruitflies (Yan et al., 2013). The data suggest that the p.M412K mutation must be critical for determining permeation properties. Amino acid 412 is part of a 50 amino acid extracellular loop between the third and fourth transmembrane domains. Whether this residue is part of a vestibule at the mouth of the pore that helps determine permeation properties or provides critical stability for the pore region remains to be determined.

The dramatically larger unitary currents and calcium permeability we measured in hair cells that express a single allele of *Tmc2* extend our observations to include TMC2 as an additional pore-forming subunit. Either subunit is capable of mediating hair cell mechanotransduction. Yet, when coexpressed, as in wild-type cochlear hair cells during the first postnatal week or in exogenous expression experiments in vestibular hair cells, the data support the hypothesis that TMC1 and TMC2 can heteromultimerize to provide a range of biophysical properties. We propose that hair cells regulate expression and assembly of TMC1 and TMC2 to help tune the properties of mechanotransduction to meet the specific needs of the inner ear organs and tonotopic regions they subserve. Developmental and tonotopic gradients in *Tmc* expression (Kawashima et al., 2011) may contribute to heteromeric TMC assemblies with a variety of stoichiometries. For example, if TMC1 and TMC2 form homo- or heterotrimeric channels, at least four subunit compositions are possible, consistent with the four discrete conductance levels we identified in WT inner hair cells. Further heterogeneity in mechanosensory transduction may arise from expression of *Tmc1* alternate splice forms, expression of other *Tmc* genes, or coassembly with other transduction molecules, perhaps TMHS (Xiong et al., 2012). Whether TMHS interacts directly with TMC1 or TMC2 to modulate hair cell transduction or affects transduction indirectly via a structural mechanism required for normal hair bundle morphogenesis has not been determined. However, we note that *Tmc1*$^{\Delta/\Delta}$;*Tmc2*$^{\Delta/\Delta}$ inner hair bundles have normal morphology but no transduction at early postnatal stages (Kawashima et al., 2011), whereas TMHS mutants have dysmorphic bundles at early postnatal stages (Xiong et al., 2012), consistent with a structural role for TMHS.

TMC1 and TMC2 have now satisfied three important criteria (Christensen and Corey, 2007; Arnadóttir and Chalfie, 2010) to be considered bona fide mechanotransduction channels. First, the onset of *Tmc2* expression coincides with development of hair cell mechanotransduction and exogenous fluorophore-tagged TMC proteins can be localized to the tips of hair cell stereocilia (Kawashima et al., 2011). Second, genetic deletion of *Tmc1* and *Tmc2* eliminates hair cell mechanosensitivity and reintroduction of exogenous *Tmc1* or *Tmc2* can restore mechanotransduction (Kawashima et al., 2011). Fulfillment of the third and most definitive criterion (Christensen and Corey, 2007) supports a direct role in mechanotransduction (Arnadóttir and Chalfie, 2010): as shown here, a point mutation in TMC1 alters the permeation properties of transduction channels in native sensory cells. We are unaware of any mutation in a protein that alters the permeation properties of a channel, unless the mutated protein is part of the channel itself. It is not surprising that a fourth criterion, reconstitution of mechanotransduction in a heterologous system, has not yet been successful. However, a recent report has shown that heterologous expression of *C. elegans tmc-1* generates Na^+-sensitive currents (Chatzigeorgiou et al., 2013), which provides further evidence that the *Tmc* superfamily includes genes that encode ion channels. Taken together, our data provide strong evidence supporting the conclusion that TMC1 and TMC2 are components of the hair cell

mechanotransduction channel. More broadly, the data present *Tmc1* and *Tmc2* as founding members of a mammalian gene family (*Tmc1–8*) that may encode multiple novel mechanosensitive ion channels.

EXPERIMENTAL PROCEDURES

Genotyping of *Tmc* Mutant Mice

Genomic DNA was prepared with Proteinase K (final concentration 1 mg/ml) and a Tail Lysis reagent (Viagen). One hundred fifty microliters of the mixture of Proteinase K and Lysis reagent was added per sample, and tubes were incubated overnight at 55°C. Once digestion was complete, the temperature was increased to 85°C for 50 min. For each sample, two separate PCR reactions were set up; one for *Tmc1*, and one for *Tmc2*. All reactions were prepared using GoTaq Green Master Mix 2X (Promega) with 2 μl of genomic DNA and four primers per gene (final concentration 0.2 nM each). Both PCR reactions were performed at 95°C for 2 min, (95°C for 30 s, 56°C for 30 s, 72°C for 45 s) × 35 cycles, 72°C for 5 min, hold at 4°C. Primers Tmc1Exon9L2 (5′-GATGAACATTTTGGTACCCTTCTACTA-3′) and Tmc1Exon9R2 (5′-CACACTTTGACACGTACAGTCTTTTAT-3′) specifically amplified a 557-base pair fragment of the wild-type *Tmc1* allele. Primers Tmc1KO5′ConfF2 (5′-TCTGAGCTTCTTAATCTCTGGTAGAAC-3′) and Tmc1KO5′ConfR2 (5′-ATACAGTCCTCTTCACATCCATGCT-3′) amplified a 408 base pair fragment of the targeted deletion allele of *Tmc1*. Primers Tmc2-7L08 (5′-CGGTTCTTCTGTGGCATCTTACTT-3′) and Tmc2-7R08 (5′-ACCAGGCAATTGACATGAATA-3′) amplified a 401 base pair fragment of wild-type *Tmc2*. Tmc2KO5′L08 (5′-CTGCCTTCTGGTTAGATCACTTCA-3′) and Tmc2KO5′R08 (5′-GTGTTTTAAGTGTACCCACGGTCA-3′) amplified a 621 base pair fragment of the targeted deletion allele of *Tmc2*. To genotype $Tmc1^{Bth}$ mice PCR reactions were set up as described above. BthMutF2 (5′-CTAATCATACCAAGGAAACATATGGAC-3′) and BthMutR2 (5′-TAGACTCACCTTGTTGTTAATCTCATC-3′) were used to amplify a 376 base pair product which was purified and sequenced.

Quantitative RT-PCR Analysis

Four mouse cochleas of each genotype were excised at P5. We divided the cochleas into equivalent basal and apical quarters. RNA was extracted, quality examined using an Agilent Bioanalyzer (Agilent Technologies) and reverse transcribed into cDNA for quantitative RT-PCR analysis with primer sets specific to *Tmc1* as described (Kawashima et al., 2011). To amplify a fragment of *Tmc1* common to both *Tmc1ex1* and *Tmc1ex2* and the $Tmc1^{Bth}$ allele, we used primers 5′-CATCTGCAGCCAACTTTGGTGTGT-3′ and 5′-AGAGGTAGCCGGAAATTCAGCCAT-3′. Primers were designed to span introns. Expression levels were normalized to those of *Actb* (β-actin) amplified with 5′-TGAGCGCAAGTACTCTGTGTGGAT-3′ and 5′-ACTCATCGTACTCCTGCTTGCTGA-3′. Primers were validated using melt curve analysis and negative controls that lacked reverse transcriptase.

Auditory Brainstem Responses

Auditory brainstem response (ABR) thresholds were measured at 30 days of age in at least four mice of each genotype: $\boldsymbol{Tmc1^{+/\Delta}}$;$Tmc2^{\Delta/\Delta}$ and $\boldsymbol{Tmc1^{Bth/\Delta}}$;$Tmc2^{\Delta/\Delta}$. We used alternating polarity tone-burst stimuli of 5 ms duration. Stimulus intensities were initiated at suprathreshold values and initially decreased by 10 dB steps, which were followed by 5 dB steps to determine the ABR threshold. When no ABR waveform was detectable at the highest stimulus level of 80 dB sound pressure level (SPL), the threshold was considered to be 85 dB SPL.

Hair Cell Counts

Organ of Corti specimens were dissected, fixed in 4% paraformaldehyde for two hours at room temperature, and decalcified in 0.25% EDTA overnight at 4°C. Samples were permeabilized with 0.5% Triton X-100 in PBS, followed by overnight incubation in the primary antibody: Anti-Myosin VI antibody produced in rabbit (Sigma-Aldrich) at 4°C and detected by an Alexa 488-conjugated to a goat anti-rabbit secondary antibody (Invitrogen). Filamentous actin was labeled with Alexa Fluor 568 phalloidin (Invitrogen). Inner hair cells were counted in a central segment of each of two regions at the basal and apical end. Each segment contained a sum total of 80 hair cell positions/row with an intact, degenerated, or lost hair cell. Hair cells were counted in 5-8 cochleas for each genotype at 4–5 weeks of age.

Scanning Electron Microscopy

Samples were prepared from C57BL/6J wild-type mice using the OTOTO method with modifications as described (Kawashima et al., 2011). Otic capsules were fixed in 2.5% glutaraldehyde buffered with 0.1 M sodium cacodylate containing 2 mM $CaCl_2$ for 1 to 1.5 hr at 4°C, rinsed in 0.1 M sodium cacodylate buffer containing 2 mM $CaCl_2$, and postfixed with 1% osmium tetroxide (OsO_4) with 0.1 M sodium cacodylate containing 2 mM $CaCl_2$ for 1 hr at 4°C. Cochlear sensory epithelia were dissected, and the tectorial membrane was removed in 70% ethanol. The tissue was hydrated to distilled water, treated with saturated aqueous thiocarbohydrazide (TCH) for 20 min, rinsed with distilled water, and immersed in 1% OsO_4 for 1 hr. After six washes with 0.1 M sodium cacodylate buffer, the TCH and OsO_4 treatments were repeated twice. The tissue was then gradually dehydrated in an ethanol series, critical point-dried, and imaged with a Hitachi S-4800 field emission electron microscope at 1 to 10 kV.

Hair Cell Electrophysiology

Utricles and cochleas were excised, mounted on glass coverslips and viewed on an Axioskop FS upright microscope (Carl Zeiss) equipped with a 63× water-immersion objective and differential interference contrast optics. Electrophysiological recordings were performed at room temperature (22°C–24°C) in standard solutions containing (in mM): 137 NaCl, 5.8 KCl, 10 HEPES, 0.7 NaH_2PO_4, 1.3 $CaCl_2$, 0.9 $MgCl_2$, and 5.6 D-glucose, vitamins (1:100), and amino acids (1:50) as in MEM (Invitrogen) (pH 7.4; 311 mOsm/kg). For some experiments, extracellular calcium was altered as indicated. Recording electrodes (3–5 MΩ) were pulled from R-6 glass (King Precision Glass) and filled with (in mM): 140 CsCl, 5 EGTA-KOH, 5 HEPES, 2.5 Na_2ATP, 3.5 $MgCl_2$, and 0.1 $CaCl_2$ (pH 7.4; 284 mOsm/kg). The whole-cell, tight-seal technique was used to record mechanotransduction currents using an Axopatch 200B (Molecular Devices). Cells were held at –84 mV unless noted otherwise. The input resistance of 12 representative cells was 885 ± 312 MΩ. Currents were filtered at 2–5 kHz with a low-pass Bessel filter, digitized at ≥20 kHz with a 12-bit acquisition board (Digidata 1322A or 1440A), and recorded using pClamp 10 software (Molecular Devices). Inner hair bundles were deflected using stiff glass probes mounted on a PICMA chip piezo actuator (Physik Instruments) driven by an LPZT amplifier (Physik Instruments) and filtered with an 8-pole Bessel filter at 40 kHz to eliminate residual pipette resonance as previously described (Stauffer and Holt, 2007). Pipettes were designed to fit into the concave aspect of the array of inner hair cell stereocilia for whole-bundle recordings or were pulled to a fine tip (~200 nm diameter) for deflecting a single stereocilium (Figure S4).

Adenoviral Vectors

The coding sequences of *Tmc1* or *Tmc2* were subcloned into the multiple cloning site of a shuttle vector with a fragment of the *MYO7A* promoter (GenBank accession # U34227 c. −46 to −3321) as described (Kawashima et al., 2011). The vectors also contained a cytomegalovirus promoter-driven sequence encoding RFP that served as a transfection marker. The resultant plasmid was linearized by digestion with PmeI and cotransformed into *E. coli* (BJ5183) cells with the adenoviral backbone plasmid, pAdEΔpol (Hodges et al., 2000). Recombinants were selected for kanamycin resistance, and recombination was confirmed by restriction endonuclease analyses. Linearized recombinant plasmids were transfected into C7 cells, an adenovirus packaging cell line (Amalfitano et al., 1998). For large-scale production, we used serial amplification of crude cell lysate in C7 cells. After five rounds of serial passage, the crude lysate was filtered and purified using an AdenoX viral purification kit (BD Biosciences) to yield ~2 ml each of Ad-*Tmc1* or Ad-*Tmc2*, at titers that ranged from 10^7 to ~10^9 viral particles/ml, which was distributed into 25-μl aliquots and stored at −80°C. Viral vectors were added directly to organotypic cultures generated from utricles of $\boldsymbol{Tmc1^{+/\Delta}}$;$Tmc2^{\Delta/\Delta}$ mice. Final working titers ranged from 2.5 × 10^6 to 10^8 viral particles/ml for 4 to 24 hr. The media was replaced with virus-free MEM supplemented with

2% BSA. Cultures were maintained for an additional 2 to 4 days before recording.

Statistics

Student's (two-tailed) t test and one-way ANOVA was used to compare ABR thresholds and biophysical properties of mechanotransduction currents using the statistical function in Origin7.5 (OriginLab). Statistical significance is indicated as $^{*}p < 0.05$, $^{**}p < 0.01$, $^{***}p < 0.001$. Data are presented as mean ± 1 standard deviation unless otherwise noted. To analyze single-channel conductances in wild-type cells (Figure 5D) we used three statistical tests, cubic clustering criterion, pseudo F statistics, and pseudo T-squares statistics, which are components of SAS 9.2 software (SAS Institute Inc).

Study Approval

All animal experiments and procedures were performed according to protocols approved by the Animal Care and Use Committee of the National Institute on Deafness and Other Communication Disorders and the Animal Care and Use Committee of Boston Children's Hospital (Protocol #1959 and #2146).

SUPPLEMENTAL INFORMATION

Supplemental Information includes six figures and can be found with this article online at http://dx.doi.org/10.1016/j.neuron.2013.06.019.

ACKNOWLEDGMENTS

We thank Erin Child for technical assistance, Lin Huang for assistance with statistical analysis, and Martin Hrabé de Angelis and Helmut Fuchs for providing *Beethoven* mice. We thank John Assad, David Clapham, David Corey, Tom Friedman, Matt Kelley, Tom Schwarz, and Clifford Woolf for helpful discussions and critical review of an earlier version of the manuscript. This work was supported by NIDCD intramural research funds Z01-DC000060-10 (A.J.G.); NIH grants R01-DC05439 (J.R.H.) and R01-DC008853 (G.S.G.). K.K. and A.J.G. hold US Patents: 7,166,433 (Transductin-2 and Applications to Hereditary Deafness; abandoned in 2009), 7,192,705 (Transductin-1 and Applications to Hereditary Deafness), and 7,659,115 (Nucleic Acid Encoding Human Transductin-1 Polypeptide). These patents have never been licensed and generate no income or royalties. B.P. collected all electrophysiology data from inner hair cells and helped analyze data. G.S.G. collected electrophysiology data from vestibular hair cells and helped analyze the data. G.C.H. collected electrophysiology data from vestibular hair cells, performed ABRs, and helped analyze data. Y.A. generated adenoviral vectors and performed qRT-PCR experiments. K.K. generated *Tmc* constructs. K.I. performed cell count analysis of *Tmc1* mutant mice. Y.K. acquired SEM images of hair cells. A.J.G. contributed to conception of the study and provided critical comments on the data and manuscript. J.R.H. conceived and designed the experiments, analyzed the data, generated the figures, and wrote the paper. All authors provided comments and approved the final submission of the manuscript.

Accepted: June 11, 2013
Published: July 18, 2013

REFERENCES

Amalfitano, A., Hauser, M.A., Hu, H., Serra, D., Begy, C.R., and Chamberlain, J.S. (1998). Production and characterization of improved adenovirus vectors with the E1, E2b, and E3 genes deleted. J. Virol. *72*, 926–933.

Arnadóttir, J., and Chalfie, M. (2010). Eukaryotic mechanosensitive channels. Annu. Rev. Biophys. *39*, 111–137.

Assad, J.A., and Corey, D.P. (1992). An active motor model for adaptation by vertebrate hair cells. J. Neurosci. *12*, 3291–3309.

Beurg, M., Evans, M.G., Hackney, C.M., and Fettiplace, R. (2006). A large-conductance calcium-selective mechanotransducer channel in mammalian cochlear hair cells. J. Neurosci. *26*, 10992–11000.

Beurg, M., Fettiplace, R., Nam, J.H., and Ricci, A.J. (2009). Localization of inner hair cell mechanotransducer channels using high-speed calcium imaging. Nat. Neurosci. *12*, 553–558.

Chatzigeorgiou, M., Bang, S., Hwang, S.W., and Schafer, W.R. (2013). tmc-1 encodes a sodium-sensitive channel required for salt chemosensation in C. elegans. Nature *494*, 95–99.

Christensen, A.P., and Corey, D.P. (2007). TRP channels in mechanosensation: direct or indirect activation? Nat. Rev. Neurosci. *8*, 510–521.

Corey, D.P., and Hudspeth, A.J. (1983). Kinetics of the receptor current in bullfrog saccular hair cells. J. Neurosci. *3*, 962–976.

Crawford, A.C., Evans, M.G., and Fettiplace, R. (1991). The actions of calcium on the mechano-electrical transducer current of turtle hair cells. J. Physiol. *434*, 369–398.

Denk, W., Holt, J.R., Shepherd, G.M., and Corey, D.P. (1995). Calcium imaging of single stereocilia in hair cells: localization of transduction channels at both ends of tip links. Neuron *15*, 1311–1321.

Eatock, R.A., Corey, D.P., and Hudspeth, A.J. (1987). Adaptation of mechanoelectrical transduction in hair cells of the bullfrog's sacculus. J. Neurosci. *7*, 2821–2836.

Esterberg, R., Hailey, D.W., Coffin, A.B., Raible, D.W., and Rubel, E.W. (2013). Disruption of intracellular calcium regulation is integral to aminoglycoside-induced hair cell death. J. Neurosci. *33*, 7513–7525.

Farris, H.E., Wells, G.B., and Ricci, A.J. (2006). Steady-state adaptation of mechanotransduction modulates the resting potential of auditory hair cells, providing an assay for endolymph [Ca2+]. J. Neurosci. *26*, 12526–12536.

Géléoc, G.S., Lennan, G.W., Richardson, G.P., and Kros, C.J. (1997). A quantitative comparison of mechanoelectrical transduction in vestibular and auditory hair cells of neonatal mice. Proc. Biol. Sci. *264*, 611–621.

Hodges, B.L., Serra, D., Hu, H., Begy, C.A., Chamberlain, J.S., and Amalfitano, A. (2000). Multiply deleted [E1, polymerase-, and pTP-] adenovirus vector persists despite deletion of the preterminal protein. J. Gene Med. *2*, 250–259.

Holt, J.R., Gillespie, S.K., Provance, D.W., Shah, K., Shokat, K.M., Corey, D.P., Mercer, J.A., and Gillespie, P.G. (2002). A chemical-genetic strategy implicates myosin-1c in adaptation by hair cells. Cell *108*, 371–381.

Holton, T., and Hudspeth, A.J. (1986). The transduction channel of hair cells from the bull-frog characterized by noise analysis. J. Physiol. *375*, 195–227.

Jaramillo, F., and Hudspeth, A.J. (1991). Localization of the hair cell's transduction channels at the hair bundle's top by iontophoretic application of a channel blocker. Neuron *7*, 409–420.

Kang, L., Gao, J., Schafer, W.R., Xie, Z., and Xu, X.Z. (2010). *C. elegans* TRP family protein TRP-4 is a pore-forming subunit of a native mechanotransduction channel. Neuron *67*, 381–391.

Kawashima, Y., Géléoc, G.S., Kurima, K., Labay, V., Lelli, A., Asai, Y., Makishima, T., Wu, D.K., Della Santina, C.C., Holt, J.R., and Griffith, A.J. (2011). Mechanotransduction in mouse inner ear hair cells requires transmembrane channel-like genes. J. Clin. Invest. *121*, 4796–4809.

Kennedy, H.J., Evans, M.G., Crawford, A.C., and Fettiplace, R. (2003). Fast adaptation of mechanoelectrical transducer channels in mammalian cochlear hair cells. Nat. Neurosci. *6*, 832–836.

Kim, K.X., and Fettiplace, R. (2013). Developmental changes in the cochlear hair cell mechanotransducer channel and their regulation by transmembrane channel-like proteins. J. Gen. Physiol. *141*, 141–148.

Kubisch, C., Schroeder, B.C., Friedrich, T., Lütjohann, B., El-Amraoui, A., Marlin, S., Petit, C., and Jentsch, T.J. (1999). KCNQ4, a novel potassium channel expressed in sensory outer hair cells, is mutated in dominant deafness. Cell *96*, 437–446.

Kurima, K., Peters, L.M., Yang, Y., Riazuddin, S., Ahmed, Z.M., Naz, S., Arnaud, D., Drury, S., Mo, J., Makishima, T., et al. (2002). Dominant and recessive deafness caused by mutations of a novel gene, TMC1, required for cochlear hair-cell function. Nat. Genet. *30*, 277–284.

Labay, V., Weichert, R.M., Makishima, T., and Griffith, A.J. (2010). Topology of transmembrane channel-like gene 1 protein. Biochemistry *49*, 8592–8598.

Lelli, A., Asai, Y., Forge, A., Holt, J.R., and Géléoc, G.S. (2009). Tonotopic gradient in the developmental acquisition of sensory transduction in outer hair cells of the mouse cochlea. J. Neurophysiol. *101*, 2961–2973.

Lumpkin, E.A., and Hudspeth, A.J. (1995). Detection of Ca^{2+} entry through mechanosensitive channels localizes the site of mechanoelectrical transduction in hair cells. Proc. Natl. Acad. Sci. USA *92*, 10297–10301.

Marcotti, W., van Netten, S.M., and Kros, C.J. (2005). The aminoglycoside antibiotic dihydrostreptomycin rapidly enters mouse outer hair cells through the mechano-electrical transducer channels. J. Physiol. *567*, 505–521.

Marcotti, W., Erven, A., Johnson, S.L., Steel, K.P., and Kros, C.J. (2006). Tmc1 is necessary for normal functional maturation and survival of inner and outer hair cells in the mouse cochlea. J. Physiol. *574*, 677–698.

O'Hagan, R., Chalfie, M., and Goodman, M.B. (2005). The MEC-4 DEG/ENaC channel of Caenorhabditis elegans touch receptor neurons transduces mechanical signals. Nat. Neurosci. *8*, 43–50.

Ricci, A.J., and Fettiplace, R. (1997). The effects of calcium buffering and cyclic AMP on mechano-electrical transduction in turtle auditory hair cells. J. Physiol. *501*, 111–124.

Ricci, A.J., Crawford, A.C., and Fettiplace, R. (2003). Tonotopic variation in the conductance of the hair cell mechanotransducer channel. Neuron *40*, 983–990.

Rüsch, A., Kros, C.J., and Richardson, G.P. (1994). Block by amiloride and its derivatives of mechano-electrical transduction in outer hair cells of mouse cochlear cultures. J. Physiol. *474*, 75–86.

Stauffer, E.A., and Holt, J.R. (2007). Sensory transduction and adaptation in inner and outer hair cells of the mouse auditory system. J. Neurophysiol. *98*, 3360–3369.

Steel, K.P., and Barkway, C. (1989). Another role for melanocytes: their importance for normal stria vascularis development in the mammalian inner ear. Development *107*, 453–463.

Vreugde, S., Erven, A., Kros, C.J., Marcotti, W., Fuchs, H., Kurima, K., Wilcox, E.R., Friedman, T.B., Griffith, A.J., Balling, R., et al. (2002). Beethoven, a mouse model for dominant, progressive hearing loss DFNA36. Nat. Genet. *30*, 257–258.

Waguespack, J., Salles, F.T., Kachar, B., and Ricci, A.J. (2007). Stepwise morphological and functional maturation of mechanotransduction in rat outer hair cells. J. Neurosci. *27*, 13890–13902.

Wu, Y.C., Ricci, A.J., and Fettiplace, R. (1999). Two components of transducer adaptation in auditory hair cells. J. Neurophysiol. *82*, 2171–2181.

Xiong, W., Grillet, N., Elledge, H.M., Wagner, T.F., Zhao, B., Johnson, K.R., Kazmierczak, P., and Müller, U. (2012). TMHS is an integral component of the mechanotransduction machinery of cochlear hair cells. Cell *151*, 1283–1295.

Yan, Z., Zhang, W., He, Y., Gorczyca, D., Xiang, Y., Cheng, L.E., Meltzer, S., Jan, L.Y., and Jan, Y.N. (2013). Drosophila NOMPC is a mechanotransduction channel subunit for gentle-touch sensation. Nature *493*, 221–225.

Yang, T., Kahrizi, K., Bazazzadeghan, N., Meyer, N., Najmabadi, H., and Smith, R.J. (2010). A novel mutation adjacent to the Bth mouse mutation in the TMC1 gene makes this mouse an excellent model of human deafness at the DFNA36 locus. Clin. Genet. *77*, 395–398.